GPS Solutions (2022) 26:63
https://doi.org/10.1007/s10291-022-01249-9

ORIGINAL ARTICLE

Understanding the characteristic of GLONASS inter-frequency clock bias using both FDMA and CDMA signals

Fan Zhang[1] · Hongzhou Chai[1] · Linyang Li[1,2] · Min Wang[1] · Xu Feng[1] · Zhenqiang Du[1]

Received: 5 October 2021 / Accepted: 11 March 2022 / Published online: 2 April 2022

Abstract

Currently, four GLONASS-M+ satellites and two GLONASS-K1 satellites transmit CDMA signals on the G3 frequency. It is important to understand the inconsistency between the new G3 and traditional FDMA G1 and G2 signals, wherein inter-frequency clock bias (IFCB) is one of the important indexes to find the difference of triple-frequency carrier phase hardware delays. Using the geometry-free and ionospheric-free (GFIF) phase combinations and an epoch-differenced method, we use 152 globally distributed MGEX stations spanning 30 days to estimate GLONASS IFCB. GLONASS-K1 satellite R09 and GLONASS-M+ satellite R21 are selected for analysis in the experiment owing to enough G3 observations. Results indicate that the magnitudes of the multipath error and SNR on G3 frequency are noticeably smaller than those of the other two frequencies. A satellite-induced multipath error seems to exist on the G3 frequency of R21, whereas R09 has none, which needs to be quantized and modeled further. The intra-day peak-peak amplitudes of R09 and R21 IFCBs are about 0.01 and 0.2 m, while inter-day amplitudes are about 0.03 and 0.3 m, respectively; R21 is even larger than that of GPS Block-IIF satellites (about 0.2 m). The RMS and STD of the IFCB series of R09 and R21 are 0.90, 0.89 cm, and 10.56, 10.53 cm, respectively. Therefore, the IFCB errors must be carefully corrected in GLONASS G3-frequency applications. Fortunately, the IFCBs of R21 present both intra-day and inter-day sine-wave periodic variations, which may be modeled, and even well predicted in the future.

Keywords GLONASS · CDMA · Inter-frequency clock bias · Satellite-induced multipath errors · Intra-day and inter-day characteristics

Introduction

The American GPS and Russian GLONASS satellite systems continue to aim for improved services and hence are actively involved in upgrading and modernizing the systems. For GPS, new generation satellites of BLOCK IIR, IIF, and III have been launched, and the third frequency L5 was added. The characteristic of new satellites and L5 frequency have been discussed in detail, i.e., regarding uncalibrated phase delay (UPD) (Pan et al. 2020), differential code bias (DCB) (Montenbruck et al. 2014; Wang et al. 2015), inter-frequency clock bias (IFCB) (Li et al. 2015; Pan et al. 2019), and triple-frequency precise point positioning (PPP) (Elsobeiey. 2015; Deo and El-Mowafy 2016; Geng et al. 2020). GLONASS traditionally employs frequency division multiple access (FDMA) to distinguish the signals transmitting from different satellites. The GLONASS-M+ (since 2011) and GLONASS-K1 (since 2016) satellites have started sending signals using code division multiple access (CDMA), which is usually used by the other global

✉ Linyang Li
lilinyang810810@163.com

Fan Zhang
18538239574@163.com

Hongzhou Chai
chaihz1969@163.com

Min Wang
Different9@163.com

Xu Feng
370986671@qq.com

Zhenqiang Du
gnsser1996@163.com

[1] PLA Strategic Support Force Information Engineering University, Zhengzhou 450001, China

[2] School of Geodesy and Geomatics, Wuhan University, Wuhan 430079, China

navigation satellite systems (Montenbruck et al. 2017). All four GLONASS-M+ satellites, including R04, R05, R12, R21, and the two GLONASS-K1 satellites, including R09 and R26, can transmit CDMA signals on the G3 frequency.

$$\begin{cases} G^s_{r,i} = \rho^s_r + c\left(dt_r - dt^s\right) - I^s_{r,1} \cdot f_1^2/f_i^2 + m^s_r \cdot \tau_r + \lambda_i \cdot \left(d^s_{r,i} - d^s_i + N^s_{r,i}\right) + \varepsilon^s_{G_i}\ i = 1,2 \\ G^s_{r,3} = \rho^s_r + c\left(dt_r - dt^s\right) - I^s_{r,1} \cdot f_1^2/f_3^2 + m^s_r \cdot \tau_r + \lambda_3 \cdot \left(d_{r,3} - d^s_3 + N^s_{r,3}\right) + \varepsilon^s_{G_3}\ i = 3 \end{cases} \tag{1}$$

However, compared with the rich research on the modernized GPS, relatively little attention has been paid to the latest GLONASS triple-frequency observations. By forming a double-difference combination, Zaminparda et al. (2017) first found that the GLONASS G3 has a lower noise level than that of GPS; the integer ambiguity resolution and positioning using the data of the satellite pair R21-R26 were also carried out. Furthermore, Zaminpardaz et al. (2021) provided an assessment of standalone GLONASS short-baseline RTK performance using both FDMA and CDMA signals. Nevertheless, the inconsistency between the carrier phase observations of G1, G2, and G3 is of great importance, especially for undifferenced and uncombined solutions. Since ambiguities can absorb a time-invariant portion of phase hardware delays, the linear combination of the time-variant portion of phase hardware delays of G1, G2, and G3 frequencies, named IFCB, should be carefully corrected. Different from GLONASS inter-frequency bias (IFB) (Wanninger 2011), IFCB has been proved to exist in other triple-frequency GNSS systems, e.g., GPS and BDS (Pan et al. 2017a, b). Note that they are two different types of biases for GLONASS, the former is a code-related bias while the latter is phase-related in this contribution.

Currently, two methods are usually utilized to estimate IFCB. The first method applies pseudorange and carrier phase observations to estimate the L1/L2 and L1/L5 satellite clock resectively (Guo and Geng 2018). Another method utilizes the geometry-free and ionospheric-free (GFIF) phase combinations (Montenbruck et al. 2012; Pan et al. 2017a), which requires only carrier phase observations which are more suitable for GLONASS because different GLONASS satellite has different pseudorange inter-frequency bias on G1 and G2 bands.

This contribution concentrates on the estimation and analysis of GLONASS phase IFCB. The estimation methods and data processing strategies are introduced first. Then, the experiment with 30 days of observation data is carried out, and the intra-day and inter-day characteristics of IFCB are analyzed. Finally, the research findings and outlooks are summarized.

GLONASS IFCB estimation method

The raw observations of GLONASS carrier phase $G^s_{r,i}$ (unit: meter) can be expressed as

where s, r, i, and f are the satellite pseudorandom noise code (PRN) number, receiver, frequency number ($i = 1, 2$), and frequency, respectively. ρ^s_r represents the geometric distance from the satellite to the receiver, c denotes the speed of light in vacuum, and dt_r and dt^s are the receiver and satellite clock errors, respectively. $I^s_{r,1}$ denotes the ionospheric delays on the first frequency. τ_r represents the zenith wet tropospheric delay with its mapping function m^s_r. $N^s_{r,i}$ and λ_i are the integer carrier phase ambiguity and wavelength, respectively. $d^s_{r,i}$ and d^s_i are satellite-dependent carrier phase hardware delays at the receiver and satellite on G1 and G2 bands, respectively, d^s_3 and $d_{r,3}$ are phase hardware delays at the receiver and satellite on the G3 frequency. $\varepsilon^s_{G_i}$ is phase measurement noise. For GLONASS FDMA signals, the frequency (unit: MHz) is satellite-dependent and linear with channel numbers, which range from $[-7, +6]$, and the frequency of CDMA G3 signal is 1202.025 MHz.

Theoretically, the satellite phase hardware delays can be divided into time-invariant portion $\tilde{d}^s_i$ and time-variant portion δd^s_i, and the same is true for receiver phase hardware delays,

$$\begin{aligned} d^s_i &= \tilde{d}^s_i + \delta d^s_i \\ d^s_{r,i} &= \tilde{d}^s_{r,i} + \delta d^s_{r,i} \end{aligned} \tag{2}$$

As Li et al. (2012) and Fan et al. (2019) pointed out, the time-variant part of the receiver IFCB is assumed to be small enough to be ignored, and hence, only satellite IFCB is the focus in this contribution. The GFIF phase combination and its variance can be obtained (Pan et al. 2018)

$$\begin{cases} GFIF\left(G_1, G_2, G_3\right) = IF^s_{r,G1G2} - IF^s_{r,G1G3} = \overline{N}_{GFIF} + \Gamma^s_{G,r} \\ \sigma_{GFIF(G_1,G_2,G_3)} = \sqrt{\left(\alpha_{12} - \alpha_{13}\right)^2 \cdot \sigma^2_{G_1} + \left(\beta_{12}\right)^2 \cdot \sigma^2_{G_2} + \left(\beta_{13}\right)^2 \cdot \sigma^2_{G_3}} \end{cases} \tag{3}$$

where σ_{G_1}, σ_{G_2}, and σ_{G_3} are all set as 0.02 cycle (Zaminparda et al. 2017). Other parameters are shown as

$$\begin{cases} \overline{N}_{GFIF} = \left(\alpha_{12}N^s_{r,1} - \beta_{12}N^s_{r,2}\right) - \left(\alpha_{13}N^s_{r,1} - \beta_{13}N^s_{r,3}\right) \\ \qquad\qquad + \left(\alpha_{12}d^s_{r,1} - \beta_{12}d^s_{r,2}\right) - \left(\alpha_{13}d^s_{r,1} - \beta_{13}d_{r,3}\right) + \left(\alpha_{12}\tilde{d}^s_1 - \beta_{12}\tilde{d}^s_2\right) - \left(\alpha_{13}\tilde{d}^s_1 - \beta_{13}\tilde{d}^s_3\right) \\ \Gamma^s_{G,r} \quad = \left(\alpha_{12}\delta d^s_1 - \beta_{12}\delta d^s_2\right) - \left(\alpha_{13}\delta d^s_1 - \beta_{13}\delta d^s_3\right) \end{cases} \tag{4}$$

where $\alpha_{mn} = f_m^2/\left(f_m^2 - f_n^2\right)$, $\beta_{mn} = f_n^2/\left(f_m^2 - f_n^2\right)$. $\Gamma^s_{G,r}$ is the phase-specific IFCBs and defined as the difference between the satellite clocks computed with G1/G2 and the satellite clocks computed with G1/G3 (Montenbruck et al. 2012; Pan et al. 2017b). $\overline{N}_{GFIF}$ is a constant which absorbs the time-invariant phase hardware delays. IFCB (represented by $\Gamma^s_{G,r}$) can be written as

$$\Gamma^s_{G,r} = GFIF\left(G_1, G_2, G_3\right) - \overline{N}_{GFIF} \tag{5}$$

Then, the epoch difference (ED) is computed to remove $\overline{N}_{GFIF}$. The ED IFCB and its variance is

$$\begin{cases} \Delta\Gamma^s_{G,r}(t) = GFIF\left(G_1, G_2, G_3\right)^s_r(t) - GFIF\left(G_1, G_2, G_3\right)^s_r(t-1) \\ \sigma_{\Delta\Gamma^s_{G,r}} = \sqrt{2}\sigma_{GFIF(G_1,G_2,G_3)} \end{cases} \tag{6}$$

where t represents the epoch number. To conduct quality control, if $\Delta\Gamma^s_{G,r}(t) > 3\sigma_{\Delta\Gamma^s_{G,r}}$, the observations at epoch t should be removed.

Next, the multi-station weighted adjustment is utilized to obtain the satellite dependent IFCB

$$\begin{cases} \Delta\Gamma^s(t) = \dfrac{\sum_{r=1}^{n}\left(\Delta\Gamma^s_{G,r}(t)\cdot\omega^s_r\right)}{\sum_{r=1}^{n}\omega^s_r} \\ \omega^s_r = \begin{cases} 2\sin e^s_r & 10^\circ \le e^s_r < 30^\circ \\ 1 & e^s_r \ge 30^\circ \end{cases} \end{cases} \tag{7}$$

where ω^s_r is the elevation-dependent weight, e^s_r is the elevation angle, and n is the number of stations involved. For quality control, satellite arcs smaller than 10 min are removed, and satellites with an elevation angle lower than 10° are also ignored. Equal weights are set for the ED IFCB at different stations at which the satellite elevation for the same satellite angles are the same (Pan et al. 2017b).

The IFCB for satellite s at epoch k can be obtained as

$$\Gamma^s_{IF}(t) = \Gamma^s\left(t_0\right) + \sum_{j=t_0+1}^{t}\Delta\Gamma^s(j) \tag{8}$$

where $\Gamma^s\left(t_0\right)$ is the IFCB at the reference epoch t_0. In this study, the IFCB at epoch 0 (t_0) is set as 0, and thus, it introduces a common bias to all epochs. However, the bias is absorbed into the ambiguity parameter and does not influence further applications (Pan et al. 2017b).

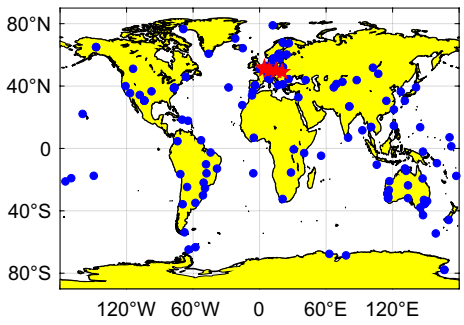

Fig. 1 Distribution of 152 MGEX stations with GLONASS triple-frequency observations used in the experiment. Blue points represent stations used to estimate IFCB, and six stations marked by red pentagrams were used to explore the characteristics of IFCB further

Table 1 List of frequency channels and satellite types of GLONASS R09 and R21 satellites

Satellite PRN	Frequency channel	Satellite type
R09	−2	GLONASS-K1
R21	4	GLONASS-M+

Table 2 Information of six stations

Station	Receiver	Antenna
BRUX	SEPT POLARX5TR	JAVRINGANT_DM
DLF1	TRIMBLE NETR9	LEIAR25.R3
FFMJ	JAVAD TRE_DELTA	LEIAR25.R3
GANP	TRIMBLE ALLOY	TRM59800.00
GOP6	SEPT POLARX5	SEPCHOKE_B3E6
GOPE	TRIMBLE ALLOY	TPSCR.G3

From (8), we know that the accuracy of IFCB estimates relies on the number of stations utilized. Therefore, tens to hundreds of stations are needed to obtain more reliable products. We note that no difference in phase IFCB estimation method exists between GLONASS and other GNSS systems. Although different GLONASS satellites send different FDMA signals, the IFCB is estimated satellite by satellite and is satellite-dependent.

Data and processing strategy

GLONASS triple-frequency observations, recorded from January 1 to 30, 2021 at 152 globally distributed stations (Fig. 1) of the IGS Multi-GNSS Experiment (MGEX) network (Montenbruck et al. 2017) are utilized to estimate the GLONASS IFCBs. Due to the unavailability of some satellites, a lack of enough observations, and usable observed arcs over the selected periods, only GLONASS-M+ satellite R21 and GLONASS-K1 satellite R09 are chosen here for analysis. Detailed information about the satellites is listed in Table 1. Six stations (Table 2) equipped with different types of receivers and antennas are used to explore the characteristics of IFCB further. All those stations are in Europe to guarantee more common satellite arcs (Fig. 1).

To take advantage of GLONASS G3 frequency, its data quality is analyzed in terms of the signal–noise ratio (SNR) and multipath error in advance. The code multipath error can be obtained as

$$M_{P_i} = P_i - \frac{f_i^2 + f_j^2}{f_i^2 - f_j^2} G_i + \frac{2f_j^2}{f_i^2 - f_j^2} G_j \tag{9}$$

As Li et al. (2019) did, we set frequency pairs obeying the following principles: if i is equal to 2 or 3, j is set as 1; if i is equal to 1, j is set as 2. The station BRUX is used to evaluate the quality of G3 frequency.

Results and discussions

The multipath error and SNR of GLONASS G3 signals are analyzed first. Then the intra-day and inter-day characteristics of the GLONASS IFCBs are investigated. Finally, the differences between the IFCBs from GLONASS-K1 satellite R09 and GLONASS-M+ satelliter21 are emphasized.

Analysis of the multipath error and SNR

Figure 2 shows the SNR values of R09 and R21 satellites at station BRUX on day of year (DOY) 001, 2021. The figure shows that the SNR values are highly related to the elevation angles. The higher the elevation angles, the larger the SNR values. Compared with GLONASS G1 and G2 bands, the G3 frequency shows the smallest SNR values, suggesting that

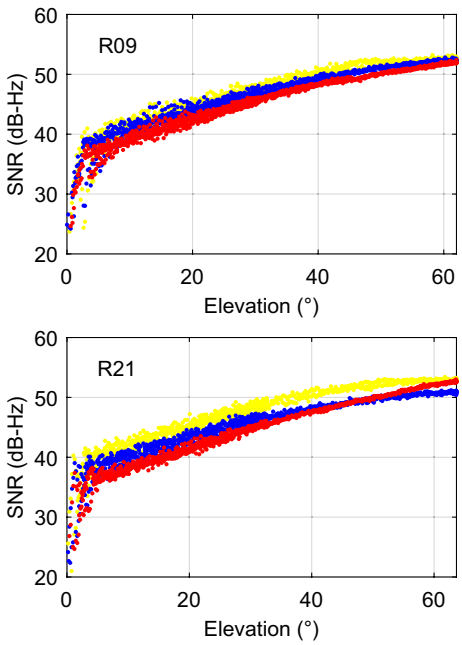

Fig. 2 SNR values of the satellite R09 (top) and R21 (bottom) for GLONASS triple-frequency signals at station BRUX on DOY 1 of 2021. G1 frequency (yellow), G2 frequency (blue), and G3 frequency (red)

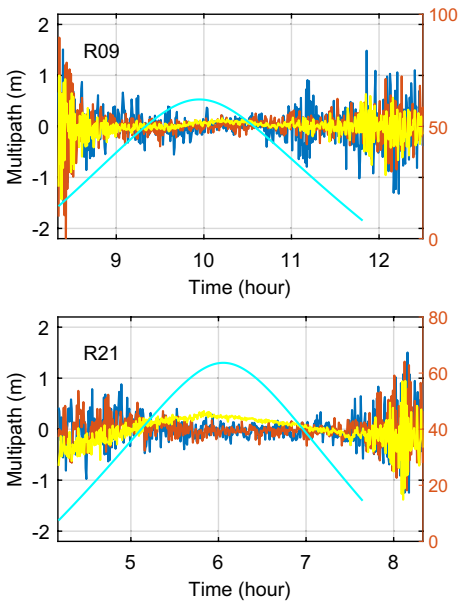

Fig. 3 Multipath error of the satellite R09 (top) and R21 (bottom) for GLONASS triple-frequency signals at station BRUX on DOY 1, 2021. G1 frequency (blue), G2 frequency (orange), G3 frequency (yellow), elevation (cyan)

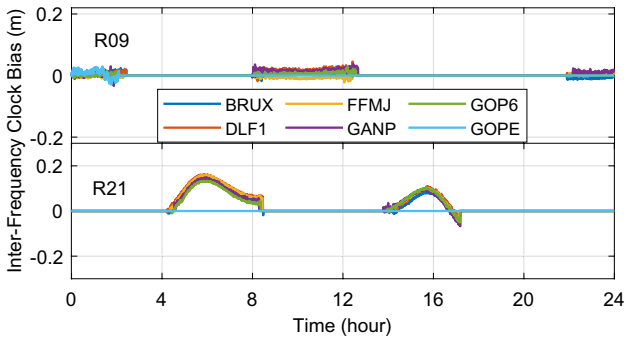

Fig. 4 Time series of the IFCB estimates at stations BRUX, DLF1, FFMJ, GANP, GOP6, and GOPE on DOY 1, 2021

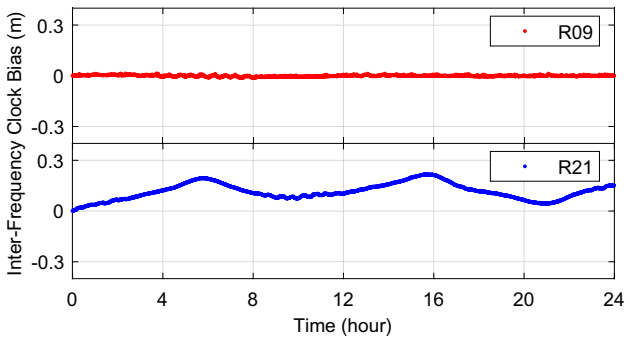

Fig. 5 Daily IFCB series of satellite R09 (top) and R21 (bottom) on DOY 1, 2021

the observation quality of the G3 frequency is lower than that of the other frequencies.

Figure 3 shows the multipath error of satellites R09 and R21. It can be concluded that the multipath value is highly related to the elevation angle. The magnitude of the multipath error on the G3 frequency is clearly smaller than that for the other two frequencies. However, similar to BDS-2 (Wanninger and Beer 2015), the satellite-induced multipath error seems to exist on the G3 frequency of the R21 satellite, while that of the R09 satellite does not exist. Similar phenomena have been observed at other R21 satellite arcs and six other stations listed in Table 2, which need further quantized and modeled. Taking SNR and the multipath error into account comprehensively, we can conclude that the quality of GLONASS G3 frequency can be further improved, especially GLONASS-M+ satellite R21.

Intra-day characteristics of GLONASS IFCB

Figure 4 shows the time series of the IFCB estimates at the six stations of Table 2 on January 1, 2021. From the figure, we know that the IFCB series of satellite R21 changes over time, which means that its IFCBs cannot be treated as daily constants, while that of R09 changes slightly. In addition, the

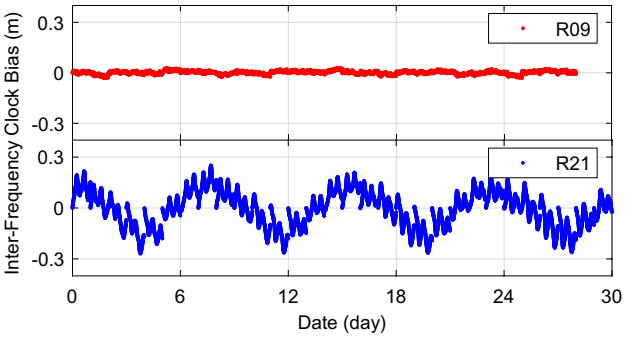

Fig. 6 IFCB series of the satellite R09 (top panel) and R21 (bottom panel) from DOY 1 to 30, 2021

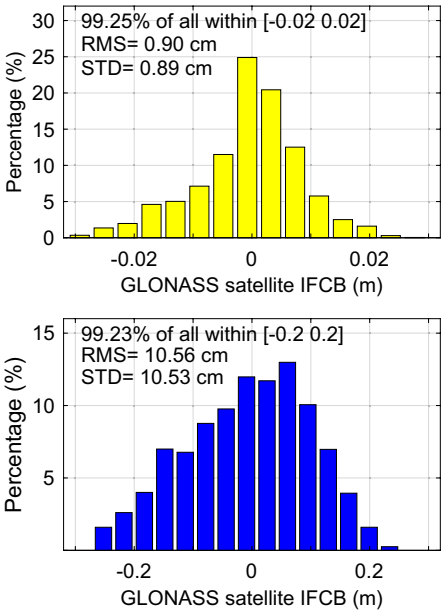

Fig. 7 Distribution of 30-days IFCBs of the satellite R09 (top) and R21 (bottom)

IFCB series are quite consistent among the six stations, suggesting that GLONASS IFCBs are satellite-dependent rather than station-dependent, which is similar to GPS Block-IIF satellites (Pan et al. 2017b).

Figure 5 shows the daily IFCB series of R09 and R21 on DOY 001, 2021. It can be seen from the figure that the IFCBs of GLONASS-K1 satellite R09 vary slightly, and their peak-peak amplitude is about 0.01 m, while those of GLONASS-M+ satellite R21 fluctuate severely, and the peak-peak amplitude reaches about 0.2 m. The IFCBs of R21 present a periodic behavior and show daily sine-wave characteristics. The possible cause is that R09 belongs to the newly launched GLONASS-K1 satellites, and R11 is a relatively old GLONASS-M+ satellite. Hence, the difference of IFCBs may originate from GLONASS satellite types.

Inter-day characteristic of GLONASS IFCB

Figure 6 shows the 30-days GLONASS IFCB series. The statistic result shows that the IFCB values of GLONASS-K1 satellite R09 fluctuate from −0.03 m to 0.03 m, while those of GLONASS-M+ satellite R21 vary from −0.3 m to 0.3 m, ten times larger than R09. Moreover, the IFCB peak-peak amplitude of R21 is even larger than that of GPS Block-IIF satellites (about 0.2 m) (Zhang et al. 2021). Additionally, similar to GPS BLOCK-IIF satellites, the IFCBs of R21 present an inter-day periodic variation, and the period should also be explored future.

To further analyze the IFCBs, Fig. 7 shows the distribution of 30-days IFCBs of R09 and R21. Through statistics, 99.25% of R09 IFCBs are smaller than 0.02 m, while 99.23% of R21 are within 0.2 m. Also, the root mean square (RMS) and standard deviation (STD) of IFCB series of R09 are 0.90 and 0.89 cm, while those of R21 are 10.56 and 10.53 cm. No systematic error has been observed for the estimated IFCBs; The RMS and STD of R21 IFCBs are more than ten times larger than those of R09, suggesting that the IFCB of GLONASS-M+ satellite R21 must be more carefully corrected in G3-frequency-related applications, whereas R09 can be ignored for their relatively small order of magnitude.

Conclusions

We estimated and analyzed the intra-day and inter-day characteristics of GLONASS IFCB based on GFIF combination and epoch-differenced method, and the IFCB characteristics of GLONASS-K1 satellite R09 and GLONASS-M+ satellite R21 are analyzed and discussed in detail. Some important findings are as follows.

1. The multipath error and SNR magnitudes on the G3 frequency are clearly smaller than those of the other two frequencies. Most importantly, the satellite-induced multipath error seems to exist on the G3 frequency of R21, while that of R09 does not exist, which needs to be quantized and modeled further.
2. The intra-day variation of R09 IFCBs is small, and its peak-peak amplitude is only about 0.01 m, while that of R21 is about 0.2 m. The inter-day peak-peak amplitude of R09 and R21 IFCBs are 0.03 and 0.3 m, respectively, and R21 is even significantly larger than that of GPS Block-IIF satellites (about 0.2 m). The RMS and STD of the IFCB series of R09 are 0.90 and 0.89 cm, while those of R21 are 10.56 and 10.53 cm, R21 is more than ten times larger than R09. Therefore, the IFCB of GLONASS-K1 satellite R21 must be more carefully corrected, while that of R09 can be ignored due to their relatively small order of magnitude. Whether this conclusion applies to the remaining one GLONASS-K1, and three GLONASS-M+ satellites should be further explored when enough observations can be accessed future.
3. Fortunately, the IFCBs of GLONASS-M+ satellite R21 present both intra-day and inter-day sine-wave periodic variations, which may be modeled, and even well predicted in the future.

Acknowledgements Thanks to MGEX for offering observation data. This study was supported by the National Natural Science Foundation of China (42074014, 42104033).

Data availability GNSS observation data are provided by Multi-GNSS Experiment (MGEX) setup by IGS. Data from MGEX are released by Institut Geographique National (IGN) that can be accessed from ftp://igs.ign.fr/pub/igs/data/campaign/mgex/daily/rinex3 and released by Bundesamt für Kartographie und Geodäsie (BKG) can be accessed from ftp://igs.bkg.bund.de/IGS/obs.

References

Deo M, El-Mowafy A (2016) Triple-frequency GNSS models for PPP with float ambiguity estimation: performance comparison using GPS. Surv Rev 50(360):249–261

Elsobeiey M (2015) Precise point positioning using triple-frequency GPS measurements. J Navig 68(3):480–492

Fan L, Shi C, Li M, Wang C, Zheng F, Jing G, Zhang J (2019) GPS satellite inter-frequency clock bias estimation using triple-frequency raw observations. J Geod 93(12):2465–2479

Geng J, Guo J, Meng X, Gao K (2020) Speeding up PPP ambiguity resolution using triple-frequency GPS/BeiDou/Galileo/QZSS data. J Geod 94(1):1–15

Guo J, Geng J (2018) GPS satellite clock determination in case of inter-frequency clock biases for triple-frequency precise point positioning. J Geod 92(10):1133–1142

Li H, Zhou X, Wu B, Wang J (2012) Estimation of the inter-frequency clock bias for the satellites of PRN25 and PRN01. Sci China Phys, Mech Astron 55(11):2186–2193

Li H, Li B, Xiao G, Wang J, Xu T (2015) Improved method for estimating the inter-frequency satellite clock bias of triple-frequency GPS. GPS Solut 20(4):751–760

Li X, Liu G, Li X, Zhou F, Feng G, Yuan Y, Zhang K (2019) Galileo PPP rapid ambiguity resolution with five-frequency observations. GPS Solut 24(1):24

Montenbruck O, Hugentobler U, Dach R, Steigenberger P, Hauschild A (2012) Apparent clock variations of the Block IIF-1 (SVN62) GPS satellite. GPS Solut 16(3):303–313

Montenbruck O, Hauschild A, Steigenberger P (2014) Differential code bias estimation using muti-GNSS observations and global ionosphere maps. Navigation 61:191–201

Montenbruck O, Steigenberger P, Prange L, Deng Z, Zhao Q, Perosanz F, Romero I, Noll C, Stürze A, Weber G (2017) The multi-GNSS experiment (MGEX) of the international GNSS service (IGS) – achievements. Prosp Chall, Adv Space Res 59(7):1671–1697

Pan L, Li X, Zhang X (2017a) Considering inter-frequency clock bias for bds triple-frequency precise point positioning. Remote Sens 9(7):734

Pan L, Zhang X, Li X, Liu J, Li X (2017b) Characteristics of inter-frequency clock bias for Block IIF satellites and its effect on

triple-frequency GPS precise point positioning. GPS Solut 21(2):811–822
Pan L, Zhang X, Li X, Liu J, Guo F, Yuan Y (2018) GPS inter-frequency clock bias modeling and prediction for real-time precise point positioning. GPS Solut 22(3):1–5
Pan L, Zhang X, Guo F, Liu J (2019) GPS inter-frequency clock bias estimation for both uncombined and ionospheric-free combined triple-frequency precise point positioning. J Geod 93(4):473–487
Pan L, Jiang X, Zhang X, Ge M, Schuh H (2020) GPS + Galileo + BeiDou precise point positioning with triple-frequency ambiguity resolution. GPS Solut 24(3):L07304-L7543
Wang N, Yuan Y, Li Z, Montenbruck O, Tan B (2015) Determination of differential code biases with multi-GNSS observations. J Geod 90(3):209–228
Wanninger L (2011) Carrier-phase inter-frequency biases of GLONASS receivers. J Geod 86(2):139–148
Wanninger L, Beer S (2015) BeiDou satellite-induced code pseudorange variations: diagnosis and therapy. GPS Solut 19(4):639–648
Zaminpardaz S, Teunissen PJG, Nadarajah N (2017) GLONASS CDMA L3 ambiguity resolution and positioning. GPS Solut 21(2):535–549
Zaminpardaz S, Teunissen PJG, Khodabandeh A (2021) GLONASS–only FDMA+CDMA RTK: performance and outlook. GPS Solut 25(3):1–12
Zhang F, Chai H, Li L, Xiao G, Du Z (2021) Estimation and analysis of GPS inter-frequency clock biases from long-term triple-frequency observations. GPS Solut 25(4):126

Fan Zhang obtained his M.S. degrees from PLA Strategic Support Force Information Engineering University, China , in 2020, where he is now a Ph.D. candidate. His research focuses on the GNSS precise positioning.

Hongzhou Chai has been a professor since 2008 and a Ph.D. supervisor since 2011 at the Zhengzhou Institute of Surveying and Mapping, China, where he received his doctorate in 2006 . His research interests include surveying data processing and GNSS positioning and navigation.

Linyang Li obtained his Ph.D. from the Institute of Surveying and Mapping, Information Engineering University, China, in 2019, where he is now a lecturer. His research focuses on the rapid processing of GNSS data.

Min Wang received his Ph.D. degree at PLA Strategic Support Force Information Engineering University in 2016 and is an associate professor from PLA Strategic Support Force Information Engineering University. His research is focused on GNSS data processing algorithm.

Xu Feng obtained his M.S degree from PLA Strategic Support Force Information Engineering University, China, in 2018, where he is now a Ph.D. candidate. His research focuses on Inertial and Geophysical Integrated Navigation.

Zhenqiang Du received his B.Sc. degree in 2018 Zhengzhou Institute of Surveying and Mapping, China, where he is currently a Ph.D. candidate. His research interests include GNSS precise point positioning and its integration with inertial navigation systems.